

Article

Surface Acidification of BiOI/TiO₂ Composite Enhanced Efficient Photocatalytic Degradation of Benzene

Ziwan Zhao¹, Hao Wang¹, Chunyu Wang¹, Yuan Sun¹, Hao Han¹, Jian Kang^{1,*}, Yanchun Dong¹ and Lei Wang^{1,2,*}

¹ State Key Laboratory of NBC Protection for Civilian, Beijing102205, China

² School of Environment, Tsinghua University, Beijing 100084, China

* Correspondence: larance0130@163.com (J.K.); wanglei16@tsinghua.org.cn (L.W.)

Abstract: A novel BiOI/TiO₂ nano-heterojunction was prepared using hydrothermal and sol-gel methods. The composite material was characterized by X-ray diffraction, ultraviolet-visible diffuse reflection spectroscopy, scanning electron microscopy, and transmission electron microscopy. The crystallinity and response to light of BiOI/TiO₂ were controlled by preparation conditions such as the optimal solvent condition and heat treatment temperature. The photocatalytic activity of the BiOI/TiO₂ catalyst was examined using benzene as a test molecule. The benzene degradation rate of the composite catalyst under visible light was enhanced compared to pure TiO₂, thus reaching 40% of the original benzene concentration, which increased further to >60% after surface acidification. The fluorescence spectra, light current, and electron paramagnetic resonance confirmed that the enhanced activity was attributed to carrier separation by the heterojunction. The acid sites and active chlorine of hydrochloric acidification offer a novel mechanism for photocatalytic reactions.



Citation: Zhao, Z.; Wang, H.; Wang, C.; Sun, Y.; Han, H.; Kang, J.; Dong, Y.; Wang, L. Surface Acidification of BiOI/TiO₂ Composite Enhanced Efficient Photocatalytic Degradation of Benzene. *Separations* **2022**, *9*, 315. <https://doi.org/10.3390/separations9100315>

Academic Editors: Yunqiao Zhou, Sheng Zhang, Bin Shi and Yueqing Zhang

Received: 27 September 2022

Accepted: 14 October 2022

Published: 17 October 2022

Publisher's Note: MDPI stays neutral with regard to jurisdictional claims in published maps and institutional affiliations.



Copyright: © 2022 by the authors. Licensee MDPI, Basel, Switzerland. This article is an open access article distributed under the terms and conditions of the Creative Commons Attribution (CC BY) license (<https://creativecommons.org/licenses/by/4.0/>).

Keywords: BiOI; heterojunction; TiO₂; visible light catalysis

1. Introduction

Recently, pollution-free photocatalytic oxidation has attracted considerable attention and recognition to resolve the limitations of environmental pollution [1–3] and energy shortage [4,5]. Gas phase degradation has always been an important application of photocatalysis, which is one of the fastest and most mature applications. Currently, industrial emissions, air pollution due to interior decorations, and vehicle exhaust deteriorate air quality and threaten human health. At normal temperatures and pressures, photocatalysis can decompose volatile organic compounds [6], degrade organic pollutants [7,8], and eliminate SO₂ [9] and NO [10,11]. Many experiments have confirmed that photocatalytic reactions, represented by TiO₂, can achieve the oxidative decomposition of alkane, alkene, alcohol, ketone, aldehyde, halogenated hydrocarbon, and organic compounds with a heteroatom, which barely causes secondary pollution [12–14]. However, the low ratio of light utilization is still the greatest drawback, hindering the industrial application of photocatalytic materials. Hence, the development of visible-light responsive photocatalysts has been an important research topic [15].

Studies reported that the heterojunction of semiconductors is a practical approach for enhancing photocatalytic performance and light response. This approach can effectively promote two suitable semiconductors. In the literature, BiVO₄/TiO₂ [16], CdS/TiO₂ [17], ZnO/TiO₂ [18], WO₃/TiO₂ [19,20], and CdS@ZnIn₂S₄ [21] can extend the photo-response range of TiO₂ to visible light and induce catalytic activity. BiOX (X = Cl, Br, and I) is a new semiconductor material with unique electronic structures and favorable optical and catalytic performance. The forbidden band of BiOI is only 1.9 eV, which is far less than the 3.4 eV of BiOCl and the 2.4 eV of BiOBr. Therefore, it has more potential for enhancing light adsorption performance. Furthermore, surface acidification by HCl may

be another approach for enhancing photocatalytic performance and light response of TiO₂ series materials [22]. However, there are no reports regarding the surface acidification of BiOI/TiO₂.

Benzene is a highly carcinogenic and poisonous compound; its ring structure is relatively stable and difficult to decompose or mineralize [23]. As the most frequently researched photocatalytic material, TiO₂ produces a high rate of benzene degradation under UV light. However, TiO₂ has broad forbidden bands that cannot be activated by visible light. Furthermore, its high electron-hole recombination rate reduces photocatalytic activity. Hence, expanding the light absorption range and eliminating benzene under visible-light irradiation has been an important challenge in photocatalysis in the gas phase. Furthermore, degradation or mineralization is often used to indicate photocatalytic activity [24,25].

In this study, a solvothermal method was used to prepare BiOI. A sol-gel method was used to form a heterojunction with TiO₂ to separate photo-carriers and extend the band edge of light absorption. Through the visible light catalysis of benzene in the gas phase, this study examined the influence of hydrothermal conditions and heat treatment temperature on BiOI and composite materials. Furthermore, the surface acidification of BiOI/TiO₂ by HCl was also studied. Our paper discusses the optimizing effect of surface acidification and mechanism to provide novel ideas for practical applications.

2. Experimental

2.1. Sample Preparation

BiOI was prepared using a solvothermal method [26]. Bi(NO₃)₃•5H₂O (2 mmol, 98%, Alfa Aesar) was mixed with KI (2 mmol, 99%, Alfa Aesar) and then 60 mL of deionized water was added and stirred for 10 min. pH and solvent changes have an important influence on BiOI preparation. KOH (AR, Macklin) was then used to adjust the pH to 2, 7, and 12. Subsequently, the liquid mixture was thoroughly stirred for 1 h, then transferred to a 100 mL autoclave at 160 °C and maintained for 24 h. Sediments were taken, filtered, washed with water and alcohol, and dried at 50 °C. BiOI obtained at pHs of 2, 7, and 12 were named BIp2, BIp7, and BIp12, respectively. Moreover, when glycol (>98%, Macklin) was used as a solvent with the other steps remaining the same, the sample was called BIoh.

BiOI was impregnated with a TiO₂ colloid prepared using Huang's method [27]. After ultrasonic dispersion for 10 min and sustained stirring for 24 h, the mixed colloid was heated for solvent removal. BiOI is unstable at high temperatures [28] and can decompose to BiO during the thermal treatment and crystallization of TiO₂. The resulting xerogel was calcined at 250, 350, 450, 550, and 650 °C, for 3 h to obtain the BiOI/TiO₂ (BIT) nano-composite catalysts.

The acidification of BIT by HCl (BITH) for enhancing photocatalytic performance and light response was further studied. Surface acidification of BIT was prepared using an impregnation method: 1 g BIT powder was immersed in 1 mL concentrated hydrochloric acid, sealed, and kept in the dark for 24 h. Subsequently, it was exposed to allow it to volatilize for 12 h, washed with water, and then dried at 50 °C. The obtained material was denoted as BITH. Bare TiO₂ was prepared using the same procedure for comparison. All chemicals used in this study were reagent grade or higher.

2.2. Characterization

X-ray diffraction (XRD) (Bruker D8 Advance) patterns were obtained using CuK α radiation. X-ray photoelectron spectroscopy (Thermo ESCALAB 250) was conducted using monochromatic Al K α radiation ($E = 1486.2$ eV) at a pressure of 3.0×10^{-10} mbar. The morphology was examined by scanning electron microscopy (SEM, JSM6700F) and TEM (JEOLJEM 2010F). A Varian Cary 500 UV-Vis spectrophotometer was used to record the UV-Vis diffuse reflectance spectra. The flat band potentials (V_{fb}) of TiO₂ and BiOI samples were determined from Mott-Schottky plots using the electrochemical method [29] performed in conventional three-electrode cells (counter electrode, Pt; reference electrode, AgCl; and electrolyte, 0.2 M Na₂SO₄ solution) using an Epsilon electrochemical workstation. The

photocurrent of samples could be tested using the same apparatus. A Bruker model A300 spectrometer was used to measure the EPR spectrum and determine photo-radicals.

2.3. Tests of Photocatalytic Activity

The impact of different BIT on photocatalytic activity was assessed by measuring the benzene degradation in the gas phase using a $\varnothing 4 \text{ mm} \times 10 \text{ cm}$ quartz tube irradiated with a Xe visible-light lamp (300 mW/cm^2 , AULTT CEL-HXUV300). Furthermore, an IR reflector and a UV filter were added to limit the range of visible light (400–800 nm). All catalysts were sieved to obtain particles, 40–60 mesh in size. A bubbler containing benzene ($\sim 100 \text{ ppm}$, 99%, Alfa Aesar) was immersed in an ice-water bath and bubbled with air. The resulting stream from the bubbler was fed to 0.4 g of catalyst at a flow rate of 20 mL/min. The temperature of reactions was controlled at $30 \text{ }^\circ\text{C}$ using an air-cooling system. Both benzene concentration and CO_2 yield were determined by gas chromatography (HP4890, Agilent) using a flame ionization detector and thermal conductivity detector, respectively. The adsorption–desorption equilibrium of benzene gas on the sample was obtained after 2 h in the dark before the activity measurement.

3. Results and Discussion

3.1. pH and Solvent Influence Photocatalytic Activity of BiOI

To explore the crystal phase composition difference, all samples (Bip2, Bip7, Bip12, and Bloh) were tested using XRD. Figure 1a shows XRD patterns of BiOI prepared using the solvothermal method. The characteristic peaks of each crystal face were clear and matched the standard pattern [30]. The degree of crystallinity of BiOI slightly decreased with an increase in the pH of the aqueous solution. The ratios in crystal faces 002, 013, 004, and 005 decreased to a certain extent. Glycol was used as a solvent, and the materials showed the lowest degree of crystallinity. Only five crystal planes, 001, 012, 110, 014, and 122, were observed in the XRD pattern, demonstrating that they form the primary part of the BiOI crystal.

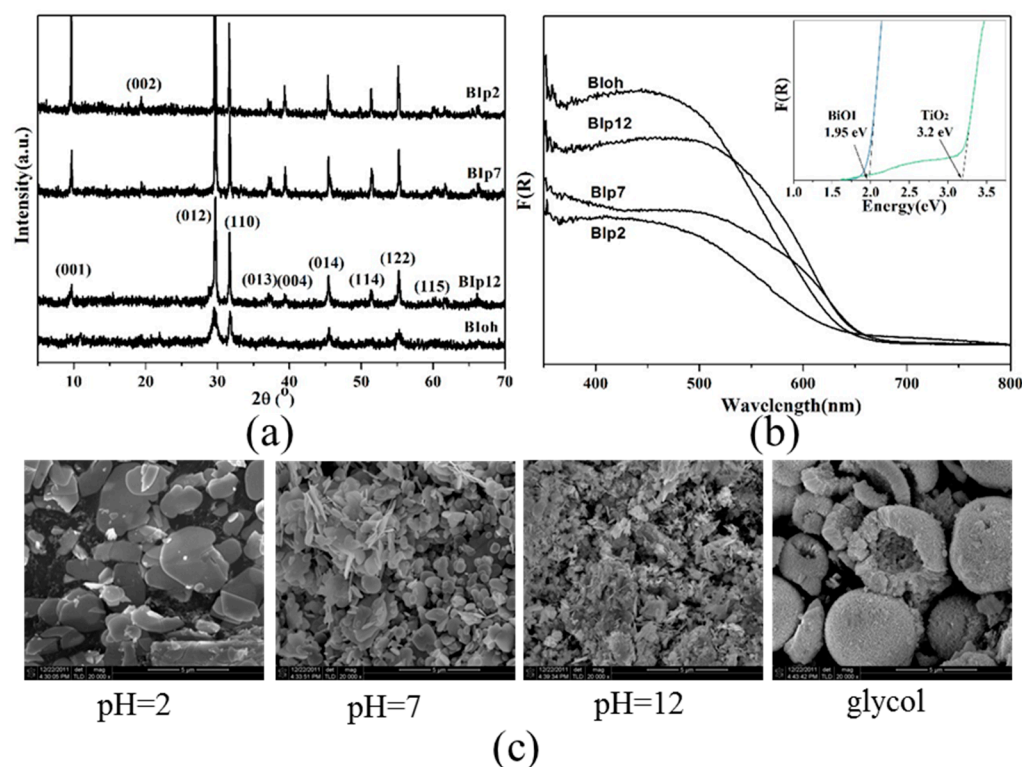


Figure 1. (a) XRD patterns, (b) UV-Vis DRS patterns, and (c) SEM images of BiOI prepared in various conditions and different solvents.

The optical absorption properties of all samples (B1p2, B1p7, B1p12, and B1oh) were tested via UV–Vis diffuse reflection spectrum. As per the UV–Vis diffuse reflection spectrum, BiOI had a wide range of light absorption. The light absorption capacity gradually increased with an increase in pH. However, the absorption edge was ~ 660 nm, and the forbidden band was estimated to be ~ 1.95 eV. The absorption band edge of B1oh demonstrated a slight blue shift, but its light absorption capacity, between 350 and 550 nm, was greater than that of BiOI prepared in the aqueous solution.

The microstructure of all samples (B1p2, B1p7, B1p12, and B1oh) was determined using SEM. As shown in Figure 1c, in strong acid, the materials exhibited lamellar structures with a maximum diameter of ~ 4 μm and a minimum of < 1 μm . At pH = 7, the BiOI lamina was significantly smaller with a maximum diameter of < 2 μm . At pH = 12, its thickness and diameter decreased to nanometer scales. A microballoon structure with a diameter of ~ 5 μm was obtained when glycol was used as a solvent for preparation. The cracked microballoon exhibited uneven surfaces that appeared to comprise nanometer lamina. Such microcosmic structures might be an important reason for the enhanced light absorption capacity of B1oh.

3.2. Characterization Analysis of BIT Prepared in Different Solvents

The composite materials of BiOI and TiO_2 were spheroidal particles, 10 nm in diameter, as shown in Figure 2a,b. The high-resolution transmission electron microscopy (TEM) images revealed 0.278 and 0.352 nm lattice fringes, corresponding to BiOI and TiO_2 , respectively. Crystallites were interconnected and evenly dispersed, thus highlighting the nano-heterojunction of BiOI/ TiO_2 . The rutile and anatase peaks of TiO_2 , in addition to the four characteristic peaks of BiOI, including crystal faces 001, 012, 110, and 014, were observed in the XRD pattern of BIT (Figure 2c,d). The introduction of BiOI caused the overall crystallinity of BIT to decrease slightly. However, the introduction of BiOI significantly increased the light absorption range from 400 nm to ~ 600 nm, thus reaching the visible light region. Accordingly, BIT displayed superior visible-light catalysis, the benzene degradation rate was $> 40\%$, and the amount of CO_2 formed was ~ 160 ppm, which was four times and two times greater, respectively, than those produced by TiO_2 . The photocatalytic activity of BIT was influenced by BiOI preparation conditions and was directly proportional to pH. Nevertheless, glycol showed better rates of benzene degradation than the aqueous solution.

3.3. Heat Treatment Impact on BIT and BiOI

Different heat treatment temperatures may influence the catalysts' BIT and BiOI structures. Figure 3a,b show the impact of the heat treatment temperature on BIT and BiOI. The results suggested that untreated samples and samples agglomerated at 250 $^\circ\text{C}$ and 350 $^\circ\text{C}$ had identical crystalline phases, which were BiOI. High temperatures increased the degree of crystallinity. When samples were heated to 450 $^\circ\text{C}$, peak patterns began to change and sharpen, which were confirmed to be $\text{Bi}_5\text{O}_7\text{I}$. This indicated that chemical changes occurred in samples. BiOI converted to Bi_2O_3 when the temperature increased to 650 $^\circ\text{C}$. Hence, BIT was the semiconductor heterojunction of BiOI and TiO_2 when the heat treatment temperature was < 350 $^\circ\text{C}$. When the temperature increased to 450 $^\circ\text{C}$, $\text{Bi}_5\text{O}_7\text{I}$, Bi_2O_3 , and TiO_2 were reported, along with BIT. The samples were completely converted to Bi_2O_3 and TiO_2 when the temperature was > 650 $^\circ\text{C}$.

Heat treatment's effect on the influence of BIT photocatalytic activity was further studied. UV–Vis DRS demonstrated that the visible-light absorption performance of pure BiOI was considerably greater than that of decomposed products (Figure 3c). The impacts of different heat treatment temperatures on BIT activity were tested under the same conditions; the results are shown in Figure 3d. The benzene degradation rate of BIT increased and then decreased with an increase in calcination temperature. The activity was optimal at 350 $^\circ\text{C}$, which was slightly higher than that at 450 $^\circ\text{C}$. At 450 $^\circ\text{C}$, the ratio of Ti ore to rutile was $\sim 4:1$; therefore, it was the optimal calcination temperature. However, BiOI started to decompose at this temperature. The visible light response of $\text{Bi}_5\text{O}_7\text{I}$ and Bi_2O_3 greatly declined. In

comparison, for BIT calcined at 350 °C, although the crystal form ratio of TiO₂ did not reach the optimal level, BiOI guaranteed the efficiency of a visible-light absorption and charge carrier activation. Hence, BIT calcined at 350 °C had a favorable catalytic performance.

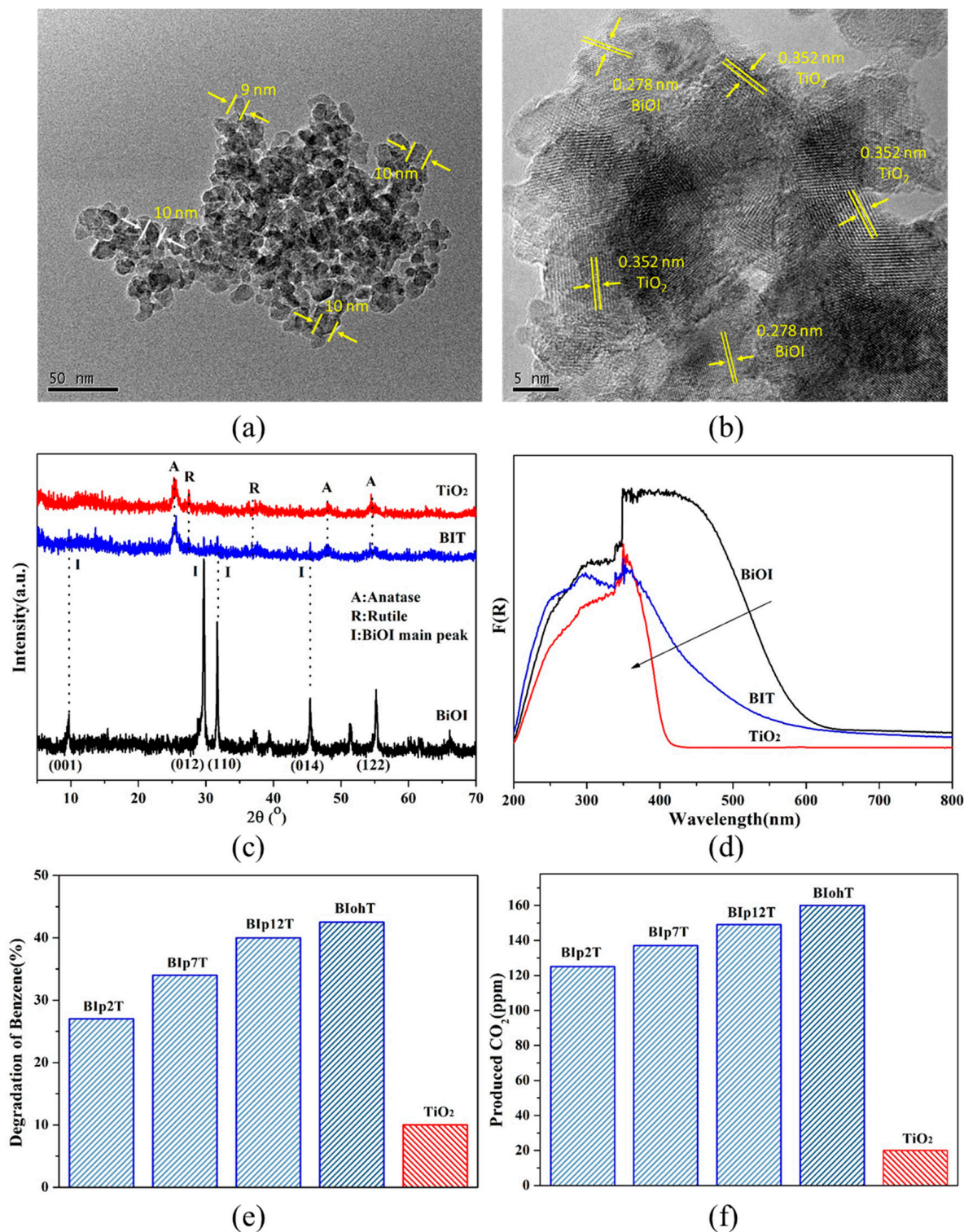


Figure 2. (a) TEM images and (b) HRTEM images of BIT; (c) XRD patterns and (d) UV-Vis DRS spectra of BIT, BiOI, and TiO₂; (e) degradation of benzene; and (f) CO₂ produced over BIT and TiO₂.

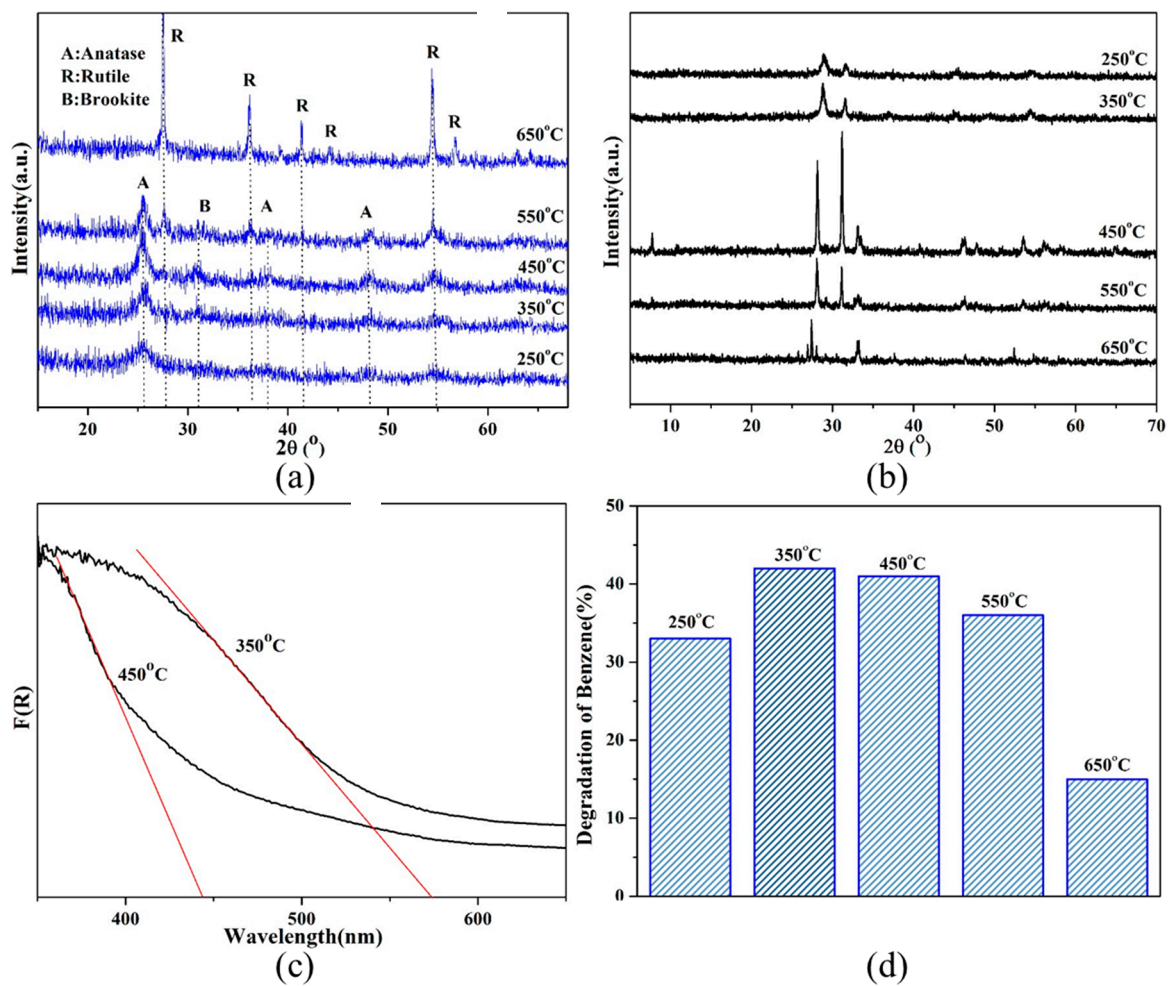


Figure 3. XRD patterns of (a) BIT and (b) BiOI; (c) UV-vis DRS patterns of BiOI; and (d) degradation of benzene over BIT calcined at different temperatures.

3.4. Surface Acidification Impact on the Photocatalytic Activity of BIT

As shown in Figure 4a,b, the promoting effect of acidification modification on BIT’s ability to degrade benzene in visible light was examined. The results demonstrated that after 10 h of illumination, BITH maintained the highest degradation rate and CO₂ production amount, which were 62% and 210 ppm, respectively. Compared to BIT, they were enhanced six times and four times that of TiO₂, respectively.

Acidification modification increased the number of acid sites on the catalyst surface and the capacity of absorbing active substances such as oxygen, water, and hydroxide radicals; thus, it has been extensively applied [31]. However, HCl dipping had a larger effect than just introducing acid sites. Cl played an important role. According to Yuan [32], Ollis [33], and Wang [22], under light conditions, Ti-based materials processed by HCl could generate Cl radicals, which achieved the oxygenolysis of organic matter molecules along with hydroxyl radicals. Figure 4c shows the photo signals generated by BITH, BIT, and TiO₂ in visible light. TiO₂ is a traditional UV light catalytic material, which involves a relatively inferior response to visible light. However, the photo-signal intensities of BITH and BIT were equivalent and much higher than TiO₂. However, BIT was attenuated in the test, whereas BITH could maintain a relatively high photocurrent intensity. Many electrons excited to conduction bands returned to valence bands (and combined with holes) and emitted energy in the form of fluorescence. Figure 4d shows the fluorescence intensity of three materials. Stronger signals indicate that photon-generated carriers possibly combined. Compared to TiO₂, BIT can more effectively transmit photon-generated carriers, thereby

separating electrons from holes and decreasing fluorescence intensity. Moreover, BITH was advantageous for charge carriers to transfer to the catalyst surface because of the larger number of acid sites and active chloride on the surface, which increased the rate of charge carrier separation. The abovementioned results conformed to its visible-light performance.

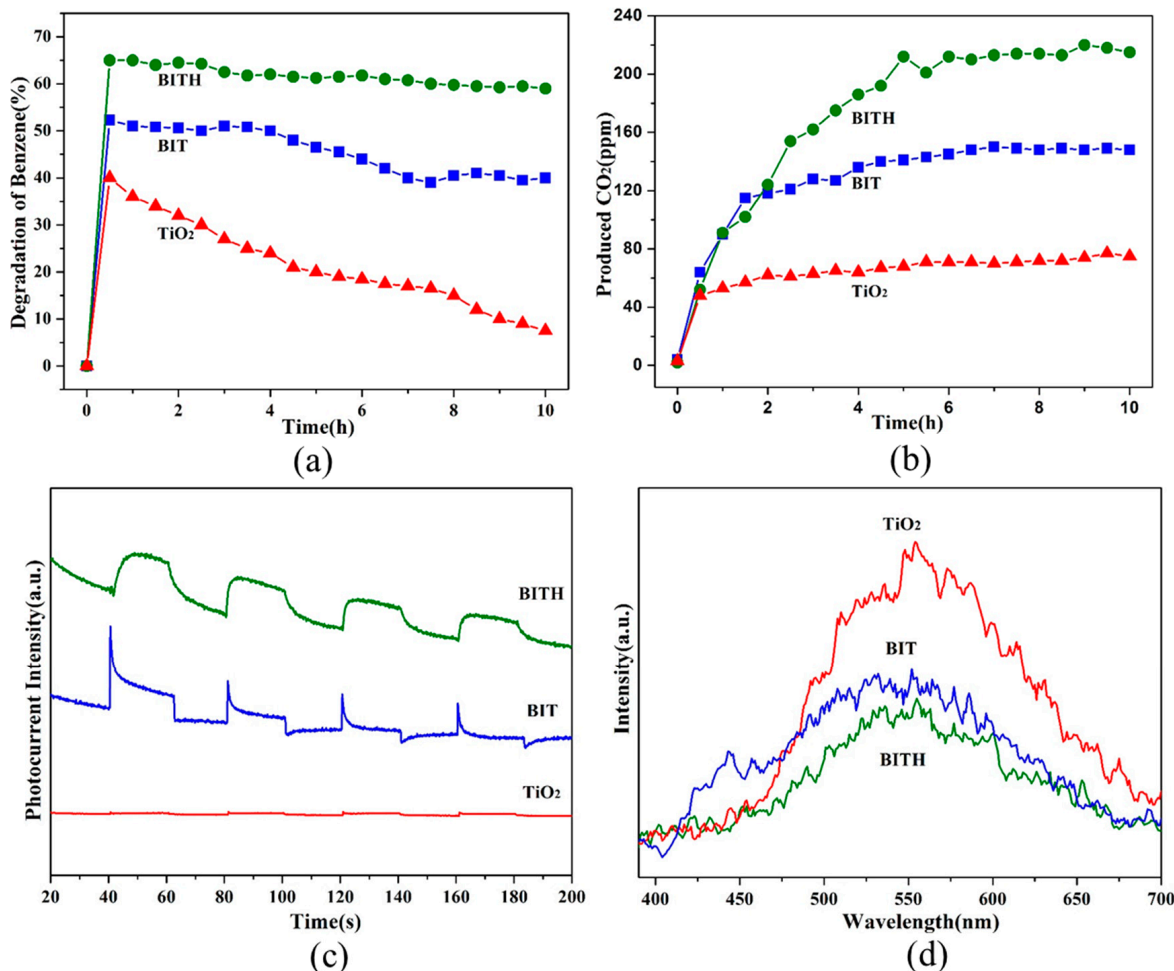


Figure 4. (a) Degradation of benzene, (b) produced CO₂, (c) photocurrent patterns, and (d) fluorescence intensity (PL) patterns of BITH, BIT, and TiO₂.

Potential produced radicals were studied further. Figure 5 shows the electron paramagnetic resonance (EPR) spectrograms of BITH and BIT under light conditions. In Figure 5a, the weak sextet was attributed to DMPO–O₂[−], which indicated that the photocatalysis system could generate superoxide radicals. In Figure 5b, the intensity ratio of the apparent quartet, 1:2:2:1, was assigned to DMPO–OH [34]. The hydroxyl radical signals of BITH and BIT were prominent, which indicated that hydroxyl radicals were the primary active species for this type of photocatalyst. However, as shown in Figure 5c, with an increase in illumination time, the typical quartet gradually weakened and disappeared in the hydroxide radical testing system of BITH. A septet appeared with an intensity ratio of 2:3:2:3:2:3:2, whereas BIT did not produce such a signal. This result was attributed to DMPO and chlorine radicals generated by chlorine under illumination. This signal was attributable to DMPOX [35]. Hence, BITH could generate novel chlorine radicals during photocatalysis and enhance benzene decomposition.

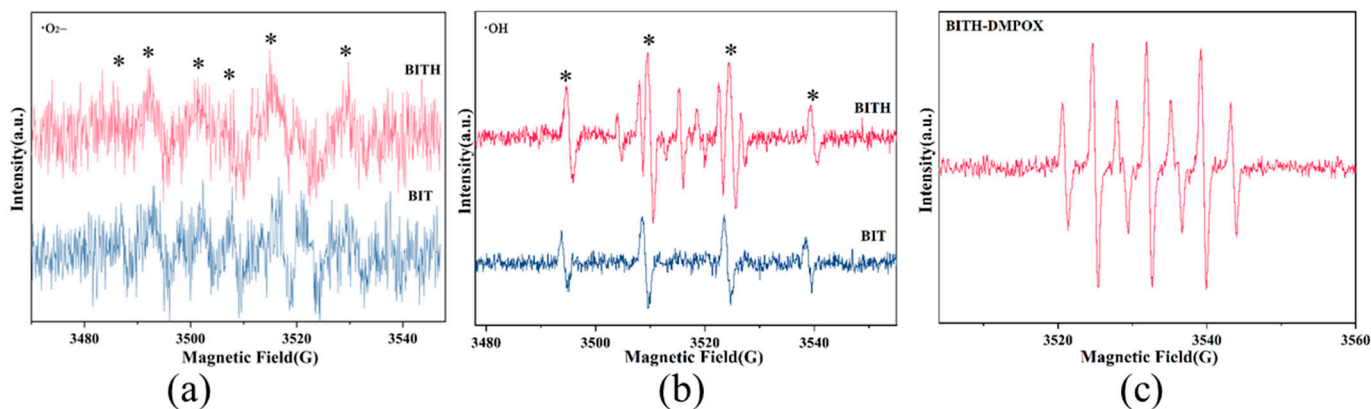


Figure 5. EPR patterns of (a) O_2^- radical, (b) OH radical over BITH and BIT, and (c) DMPOX over BITH.

3.5. Photocatalytic Mechanism of BITH

As the typical p-type semiconductor, the Fermi level of BiOI was in the lower middle part of the forbidden bands and close to the valence bands, whereas n-TiO₂ was close to the conduction band. After forming the heterojunction, the Fermi levels of two semiconductors reached the same electric potential. Changes occurred in the relative positions of conduction bands. BiOI was higher than TiO₂ and formed potential gradients, thus making electron transmission possible [36]. As shown in Figure 6, BiOI was activated when illuminated with visible light, and electrons in the valence bands migrated to the conduction bands. The electrons in BiOI valence bands then migrated to the TiO₂ conduction bands via the heterojunction, thus leading to the separation of charge carriers. The photoelectrons diffused to the catalyst surface and combined with oxygen molecules to generate superoxide radicals. However, the holes of BiOI valence bands migrated to the catalyst surface and converted the hydroxide ions or water molecules to hydroxyl radicals. With photoexcitation, chloride produced by hydrochloric acidification could generate Cl or O radicals, which promoted the broken bond oxidation of organic matter molecules; hence, BITH showed superior photocatalysis.

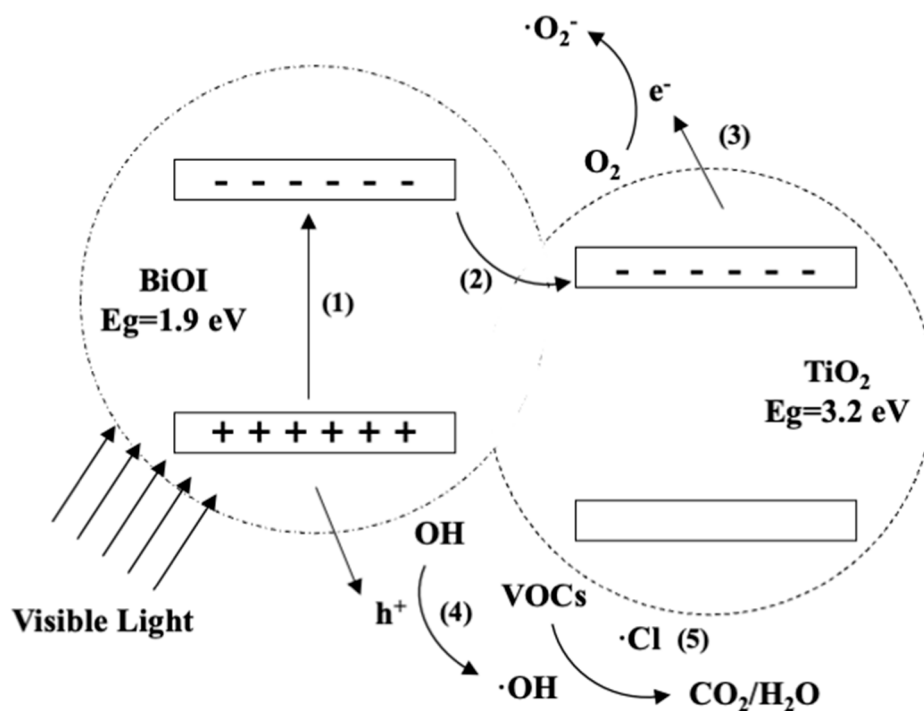


Figure 6. Mechanism of photoexcitation on the BITH heterojunction.

4. Conclusions

A BIT nanometer heterojunction with superior performance in visible light was prepared using glycol as a solvent followed by thermal treatment at 350 °C. The photocatalytic performance of BIT was further enhanced using a surface acid treatment. The benzene degradation rate was 1.5 and 6 times higher than those of BIT and pure TiO₂, respectively. These results show that a combination of BiOI and TiO₂ can increase the separation efficiency of photon-generated carriers, expand the light absorption range, and enhance photocatalytic performance. Surface acidification modification enhanced the photocatalytic activity of BiOI/TiO₂, which was ascribed to introduced acid sites and active chlorine to BIT. Our results indicated that heterojunction is a practical approach for enhancing photocatalytic performance and light response. Furthermore, surface acidification of BiOI/TiO₂ significantly enhanced photocatalytic activity, thereby providing novel ideas for relevant research.

Author Contributions: Conceptualization, J.K., Y.D. and L.W.; data curation, Z.Z. and H.W.; formal analysis, Z.Z., C.W. and L.W.; writing—original draft, Z.Z.; writing—review and editing, H.W., C.W., Y.S., H.H., J.K., Y.D. and L.W. All authors have read and agreed to the published version of the manuscript.

Funding: This research was supported by the Fundamental Research Fund from the State Key Laboratory of NBC Protection for Civilian (SKLNBC 2022-03), China.

Institutional Review Board Statement: Not Applicable.

Informed Consent Statement: Not Applicable.

Data Availability Statement: Not Applicable.

Conflicts of Interest: The authors declare that the research was conducted in the absence of any commercial or financial relationships that could be construed as a potential conflict of interest.

References

1. Xiong, L.; Tang, J. Strategies and challenges on selectivity of photocatalytic oxidation of organic substances. *Adv. Energy Mater.* **2021**, *11*, 2003216. [[CrossRef](#)]
2. Shu, Y.; Ji, J.; Zhou, M.; Liang, S.; Xie, Q.; Li, S.; Liu, B.; Deng, J.; Cao, J.; Liu, S.; et al. Selective photocatalytic oxidation of gaseous ammonia at ppb level over Pt and F modified TiO₂. *Appl. Catal. B Environ.* **2022**, *300*, 120688. [[CrossRef](#)]
3. Chen, M.; Wang, H.; Chen, X.; Wang, F.; Qin, X.; Zhang, C.; He, H. High-performance of Cu-TiO₂ for photocatalytic oxidation of formaldehyde under visible light and the mechanism study. *Chem. Eng. J.* **2020**, *390*, 124481. [[CrossRef](#)]
4. Erhuan, Z.; Jia, L.; Muwei, J.; Wang, H.; Wan, X.; Rong, H.; Chen, W.; Liu, J.; Xu, M.; Zhang, J. Hollow anisotropic semiconductor nanoprisms with highly crystalline frameworks for high-efficiency photoelectrochemical water splitting. *J. Mater. Chem. A* **2019**, *7*, 8061–8072.
5. Shafiq, I.; Hussain, M.; Shafique, S.; Rashid, R.; Akhter, P.; Ahmed, A.; Jeon, J.-K.; Park, Y.-K. Oxidative desulfurization of refinery diesel pool fractions using LaVO₄ photocatalyst. *J. Ind. Eng. Chem.* **2021**, *98*, 283–288. [[CrossRef](#)]
6. Shayegan, Z.; Haghghat, F.; Lee, C.S. Photocatalytic oxidation of volatile organic compounds for indoor environment applications: Three different scaled setups. *Chem. Eng. J.* **2019**, *357*, 533–546. [[CrossRef](#)]
7. Zhou, F.; Yan, C.; Liang, T.; Sun, Q.; Wang, H. Photocatalytic degradation of Orange G using sepiolite-TiO₂ nanocomposites: Optimization of physicochemical parameters and kinetics studies. *Chem. Eng. Sci.* **2018**, *183*, 231–239. [[CrossRef](#)]
8. Wang, D.; Jia, F.; Wang, H.; Chen, F.; Fang, Y.; Dong, W.; Zeng, G.; Li, X.; Yang, Q.; Yuan, X. Simultaneously efficient adsorption and photocatalytic degradation of tetracycline by Fe-based MOFs. *J. Colloid Interface Sci.* **2018**, *519*, 273–284. [[CrossRef](#)] [[PubMed](#)]
9. Chen, Y.; Tong, S.; Li, W.; Liu, Y.; Tan, F.; Ge, M.; Xie, X.; Sun, J. Photocatalytic oxidation of SO₂ by TiO₂: Aerosol formation and the key role of gaseous reactive oxygen species. *Environ. Sci. Technol.* **2021**, *55*, 9784–9793. [[CrossRef](#)]
10. Geng, Y.; Chen, D.; Li, N.; Xu, Q.; Li, H.; He, J.; Lu, J. Z-Scheme 2D/2D α -Fe₂O₃/g-C₃N₄ heterojunction for photocatalytic oxidation of nitric oxide. *Appl. Catal. B Environ.* **2021**, *280*, 119409. [[CrossRef](#)]
11. Li, R.; Ou, X.; Zhang, L.; Qi, Z.; Wu, X.; Lu, C.; Fan, J.; Lv, K. Photocatalytic oxidation of NO on reduction type semiconductor photocatalysts: Effect of metallic Bi on CdS nanorods. *Chem. Commun.* **2021**, *57*, 10067–10070. [[CrossRef](#)] [[PubMed](#)]
12. Cano-Casanova, L.; Mei, B.; Mul, G.; Lillo-Rodenas, M.A.; Roman-Martinez, M.D.C. Photocatalytic oxidation of propane using hydrothermally prepared anatase-brookite-rutile TiO₂ samples. An in situ drifts study. *Nanomaterials* **2020**, *10*, 1314. [[CrossRef](#)] [[PubMed](#)]
13. Mamaghani, A.H.; Haghghat, F.; Lee, C.S. Photocatalytic oxidation technology for indoor environment air purification: The state-of-the-art. *Appl. Catal. B Environ.* **2017**, *203*, 247–269. [[CrossRef](#)]

14. Diniz, J.; Nunes, C.D.; Monteiro, O.C. Novel approach to synthesise MoO₃—TiO₂ nanocomposites for the photo-assisted oxidation of benzyl alcohol to benzaldehyde. *Inorg. Chem. Commun.* **2020**, *119*, 108099. [[CrossRef](#)]
15. Carey, J.H.; Lawrence, J.; Tosine, H.M. Photodechlorination of PCB's in the presence of titanium dioxide in aqueous suspensions. *Bull. Environ. Contam. Toxicol.* **1976**, *16*, 697–701. [[CrossRef](#)]
16. Hu, Y.; Li, D.; Zheng, Y.; Chen, W.; He, Y.; Shao, Y.; Fu, X.; Xiao, G. BiVO₄/TiO₂ nanocrystalline heterostructure: A wide spectrum responsive photocatalyst towards the highly efficient decomposition of gaseous benzene. *Appl. Catal. B* **2011**, *104*, 30–36. [[CrossRef](#)]
17. Gopidas, K.P.; Bohorguez, M.; Kamat, P.V. Photophysical and photochemical aspects of coupled semiconductors: Charge-transfer processes in colloidal cadmium sulfide–titania and cadmium sulfide–silver (I) iodide systems. *J. Phys. Chem.* **1990**, *94*, 6435–6440. [[CrossRef](#)]
18. Guanyu, C.; Kaibo, Z.; Xiaoliang, M. Preparation of ZnO/TiO₂ composite nanomaterial and application in dye-sensitized solar cells. *Chin. J. Vac. Sci. Technol.* **2010**, *30*, 621–625.
19. Do, Y.R.; Lee, W.; Dwight, K.; Wold, A. The effect of WO₃ on the photocatalytic activity of TiO₂. *J. Solid State Chem.* **1994**, *108*, 198–201. [[CrossRef](#)]
20. Hu, C.C.; Nian, J.N.; Teng, H.S. Electrodeposited p-type Cu₂O as photocatalyst for H₂ evolution from water reduction in the presence of WO₃. *Sol. Energy Mater. Sol. Cells* **2008**, *92*, 1071–1076. [[CrossRef](#)]
21. Erhuan, Z.; Qianhong, Z.; Junheng, H. Visually resolving the direct Z-scheme heterojunction in CdS@ZnIn₂S₄ hollow cubes for photocatalytic evolution of H₂ and H₂O₂ from pure water. *Appl. Catal. B Environ.* **2021**, *293*, 120213.
22. Lei, W.; Jian, G.; Hao, H.; Yao, M.; Kang, J.; Peng, M.; Wang, D.; Xu, J.; Hao, J. Enhanced photocatalytic removal of ozone by a new chlorine-radical-mediated strategy. *Appl. Catal. B Environ.* **2022**, *306*, 121130.
23. Zhang, L.; Sun, P.; Sun, D.; Zhou, Y.; Han, L.; Zhang, H.; Zhu, B.; Wang, B. Occupational health risk assessment of the benzene exposure industries: A comprehensive scoring method through 4 health risk assessment models. *Environ. Sci. Pollut. Res.* **2022**, 1–12. [[CrossRef](#)] [[PubMed](#)]
24. Xu, Y.J.; Zhuang, Y.; Fu, X. New insight for enhanced photocatalytic activity of TiO₂ by doping carbon nanotubes: A case study on degradation of benzene and methyl orange. *J. Phys. Chem. C* **2010**, *114*, 2669–2676. [[CrossRef](#)]
25. He, F.; Li, J.; Li, T.; Li, G. Solvothermal synthesis of mesoporous TiO₂: The effect of morphology, size and calcination progress on photocatalytic activity in the degradation of gaseous benzene. *Chem. Eng. J.* **2014**, *237*, 312–321. [[CrossRef](#)]
26. Zhang, X.; Zhang, L. Electronic and band structure tuning of ternary semiconductor photocatalysts by self doping: The case of BiOI. *J. Phys. Chem. C* **2010**, *114*, 18198–18206. [[CrossRef](#)]
27. Huang, H.; Li, D.; Lin, Q.; Zhang, W.; Shao, Y.; Chen, Y.; Sun, M.; Fu, X. Efficient degradation of benzene over LaVO₄/TiO₂ nanocrystalline heterojunction photocatalyst under visible light irradiation. *Environ. Sci. Technol.* **2009**, *43*, 4164–4168. [[CrossRef](#)] [[PubMed](#)]
28. Chang, C.; Zhu, L.; Fu, Y.; Chu, X. Highly active Bi/BiOI composite synthesized by one-step reaction and its capacity to degrade bisphenol A under simulated solar light irradiation. *Chem. Eng. J.* **2013**, *233*, 305–314. [[CrossRef](#)]
29. Ramesham, R. Determination of flatband potential for boron doped diamond electrode in 0.5 M NaCl by AC impedance spectroscopy. *Thin Solid Films* **1998**, *322*, 158–166. [[CrossRef](#)]
30. Wang, W.; Huang, F.; Lin, X.; Yang, J. Visible-light-responsive photocatalysts xBiOBr-(1-x)BiOI. *Cat. Commun.* **2008**, *9*, 8–12. [[CrossRef](#)]
31. Martra, G. Lewis acid and base sites at the surface of microcrystalline TiO₂ anatase: Relationships between surface morphology and chemical behavior. *Appl. Catal. A Gen.* **2000**, *200*, 275–285. [[CrossRef](#)]
32. Yuan, R.S.; Chen, T.; Fei, E.H.; Lin, J.; Ding, Z.; Long, J.; Zhang, Z.; Fu, X.; Liu, P.; Wu, L.; et al. Surface chlorination of TiO₂-based photocatalysts: A way to remarkably improve photocatalytic activity in both UV and visible region. *ACS Catal.* **2011**, *1*, 200–206. [[CrossRef](#)]
33. d'Hennezel, O.; Pichat, P.; Ollis, D.F. Benzene and toluene gas-phase photocatalytic degradation over H₂O and HCl pretreated TiO₂: By-products and mechanisms. *J. Photochem. Photobiol. A* **1998**, *118*, 197–204. [[CrossRef](#)]
34. Liu, G.; Zhao, J.; Hidaka, H. ESR spin-trapping detection of radical intermediates in the TiO₂-assisted photo-oxidation of sul for rhodamine B under visible irradiation. *J. Photochem. Photobiol. A* **2000**, *133*, 83–88. [[CrossRef](#)]
35. Xianfeng, H.; Yi, W.; Xuchun, L.; Guan, D.; Li, Y.; Zheng, X.; Zhao, M.; Shan, C.; Pan, B. Autocatalytic decomplexation of Cu(II)-EDTA and simultaneous removal of aqueous Cu(II) by UV/chlorine. *Environ. Sci. Technol.* **2019**, *53*, 2036–2044.
36. Lee, S.; Dai, G.; Liang, Y.; Liu, H.; Zhang, X. Preparing BiOI/Bi₂O₃ photocatalyst with highly visible-light activity by in-situ dissolution-sedimentation. *Chin. J. Inorg. Chem.* **2011**, *27*, 1964–1968.